Journal of Alloys and Compounds 545 (2012) 90–98

Contents lists available at SciVerse ScienceDirect

Journal of Alloys and Compounds

journal homepage: www.elsevier.com/locate/jalcom

Surface morphology and depth profile study of $Cd_{1-x}Zn_xTe$ alloy nanostructures

Ercan Yilmaz [a,*], Evrin Tuğay [b,c], Aliekber Aktağ [a], Ilker Yildiz [b], Mehmet Parlak [b,c], Raşit Turan [b,c]

[a] Physics Department, Abant Izzet Baysal University, 14280 Bolu, Turkey
[b] Physics Department, Middle East Technical University, 06531 Ankara, Turkey
[c] Center for Solar Energy Research and Applications (GÜNAM), Middle East Technical University, 06531 Ankara, Turkey

ARTICLE INFO

Article history:
Received 12 February 2012
Received in revised form 5 August 2012
Accepted 7 August 2012
Available online 20 August 2012

Keywords:
CdZnTe
Sputtering
XRD
XPS
EDS
SEM
AFM

ABSTRACT

$Cd_{1-x}Zn_xTe$ thin films with thickness of 200 nm were deposited on glass substrates from a single sputtering target. During the deposition process, the substrates were heated at 400 °C and deposited films were subjected to an annealing process at 300 and 450 °C for an hour under flowing N_2 gas at atmospheric pressure. Influence of *in situ* heating and post-deposition annealing treatments on the structural and optical evolution of $Cd_{1-x}Zn_xTe$ nanostructures were investigated by diagnostic techniques such as X-ray diffraction (XRD), energy dispersive spectroscopy (EDS), scanning electron microscopy (SEM), atomic force microscopy (AFM), X-ray photoelectron spectroscopy (XPS), and UV-transmission spectroscopy. The transmission spectra in the region of the optical absorption band edge were measured for as-deposited and heat-treated of CdZnTe samples. Band gap of the deposited films were found to be in the range of 1.59–1.66 eV. The XRD studies revealed that heated $Cd_{1-x}Zn_xTe$ films have a cubic oriented (111), (220) and (311) polycrystalline structure whereas unheated films are mostly amorphous. The effects of annealing temperature on the composition of the thin films were discussed. XPS measurements were performed in the depth profiling mode in order to understand the variation in the chemical composition of the films. Results were compared with the structural analysis obtained from the XRD measurements.

1. Introduction

Cadmium based binary and ternary II–IV compound semiconductors have attracted considerable interest because of their applications in optoelectronic devices, solar cells, photo-detectors, and gamma-ray detectors [1–5]. Electronic and optical properties of $Cd_{1-x}Zn_xTe$ makes it a promising material for terrestrial photovoltaic applications [6,7]. Various methods have been used to prepare $Cd_{1-x}Zn_xTe$ films: molecular beam epitaxy [8], liquid phase epitaxy [9], electro deposition [10], close space vapor transport [11], laser ablation [12], thermal vapor evaporation [13–16], metal–organic chemical vapor deposition (MOCVD) [17] and sputtering [18]. The sputtering technique is a suitable technique for large scale applications such as the fabrication of large area solar cells. It is a flexible and low temperature process which is particularly required for the fabrication of multilayer tandem solar cells. The sputtering has been used to fabricate CdZnTe films on glass substrate using multi-target sources like CdTe target and Zn powders or CdTe and ZnTe targets [19]. Fabrication of the structure of $Cd_{1-x}Zn_xTe$ films on glass, from a single target source, is a technological interest for above mentioned applications. The major advantage of deposition from a single $Cd_{1-x}Zn_xTe$ target is providing a better uniformity and reproducibility in the deposited films. In this study, we have essentially attempted to answer the question of the structural stability of $Cd_{1-x}Zn_xTe$ during the heat treatments [20,21], and shown that uniform and stoichiometric $Cd_{1-x}Zn_xTe$ layers with required chemical compositions can be fabricated from a single $Cd_{1-x}Zn_xTe$ target.

2. Experimental details

$Cd_{1-x}Zn_xTe$ films were deposited on glass substrates at 400 °C in a radio frequency (r.f.) sputtering system. The r.f. power in the deposition process was 40 W. A single 4-inch diameter CdZnTe (99.99%) target was used. The base pressure of the sputtering chamber was 1.5×10^{-6} torr and it was kept at 5m Torr during sputtering under Ar gas. By setting sputtering parameters, the influence of the *in situ* heated substrate at 400 °C and post deposition annealing temperatures of 300 and 450 °C for 1 h in quartz tube furnace under flowing N_2 gas at atmospheric pressure on the structural and optical properties of $Cd_{1-x}Zn_xTe$ nanostructures have been studied. Growth rate was 0.3 Å/s in the deposition process. Measured films thicknesses were about 200 nm.

The crystallinity, size evolution, lattice constant (a_x), and zinc concentration (x) of the films was determined from the standard X-ray diffraction (XRD) patterns using Cu K_α radiation. The angle (2) range was from 10° to 60°. Elemental composition and surface morphology of the $Cd_{1-x}Zn_xTe$ alloys were performed by both energy dispersive X-ray spectroscopy (EDS) and scanning electron microscopy (SEM) measurements using FE-SEM (Nova NanoSEM 430) equipment. The X-ray photoelectron spectroscopy (XPS) depth profiles of as-deposited at 400 °C and annealed at 300 and 450 °C are carried out to obtain the relative elemental concentration. A Specs XPS system operating at a vacuum of 1×10^{-7} Pa was used to determine the depth profiles of Cd, Zn, Te, O, and C atoms in the sputtered layer. After four times sputtering of 2000 eV Ar^+ ions, with the cycle of 2 min followed by 4 min 3500 eV sputtering cycles, the steady state elemental composition values was

* Corresponding author. Tel.: +90 374 254 10 00/1335; fax: +90 374 253 46 42.
E-mail address: yilmaz@ibu.edu.tr (E. Yilmaz).

0925-8388/$ - see front matter © 2012 Elsevier B.V. All rights reserved.
http://dx.doi.org/10.1016/j.jallcom.2012.08.028

obtained for each element. To acquire the details of the $Cd_{1-x}Zn_xTe$ alloys surface morphology and their evolution by annealing treatments, AFM measurements have been performed.

For the optical characterization, normal incidence reflectance R and transmittance T were determined by Shimadzu UV-360 spectrometer in the wavelength range of 350–900 nm at room temperature. In the range of strong absorption of the radiation, the absorption coefficient has been calculated from the relation [2]; $\alpha = (1/d)\ln(100/T)$ where T is the transmittance and d is the thickness of the film. Nearly linear related part of $(\alpha h\nu)^{1/2}$ vs. $h\nu$ plots for films of different composition indicates the direct band gap nature of the films. Extrapolation of the line to the $h\nu$ axis specifies a direct band gaps in the range of 1.59–1.66 eV.

3. Results and discussions

3.1. XRD measurements

X-ray diffraction (XRD) studies were carried out on $Cd_{1-x}Zn_xTe$ alloy samples and the spectra were analyzed to obtain information about various crystallographic aspects including crystallinity, size evolution, lattice constant (a_x), and zinc concentration (x). The experimental lattice constant (a_x) for $Cd_{1-x}Zn_xTe$ alloy can be obtained from the Bragg's relation $2d_{hkl}\ sin(\theta) = n\lambda$, by taking θ values from the peaks of XRD patterns. The zinc concentration (x) for this ternary compound can be determined by the Vegard's law: $a(Cd_{1-x}Zn_xTe) = (1-x)\ a(CdTe) + a(ZnTe)$, assuming that a linear relation exists between the crystal lattice constant of the $Cd_{1-x}Zn_xTe$ alloy and the concentrations of the constituent elements, at constant temperature [20]. Fig. 1(a) shows the annealing temperature evolution XRD spectra of the $Cd_{1-x}Zn_xTe$ alloy samples prepared at substrate temperature of 400 °C and post annealed at 300 and 450 °C. Three main diffraction peaks, which vary with x value, appeared at ~24°, ~40°, and ~47° have been identified corresponding to (1 1 1), (2 2 0) and (3 1 1) diffraction peaks. The XRD patterns were offset to show the diffraction peaks clearly. All samples even the as-deposited one show polycrystalline structure and mostly preferred [1 1 1] orientation. For all $Cd_{1-x}Zn_xTe$ alloys, the most intense peak is (1 1 1) diffraction and the corresponding lattice constant (a_x) locates between that of CdTe (6.4810 Å) [JCPDS file No. 15-0770] and ZnTe (6.1026 Å) [JCPDS file No. 15-0746]. Fig. 1(b) shows the exact position and the relative intensity of the (1 1 1) diffraction for three samples. By increasing annealing temperature up to 450 °C, the diffraction peaks become more tinny and intense indicating improved crystallinity of the alloy and enhanced coalescening between the grains leading to the formation of larger grains. By applying the Scherrer formula, $t = K\lambda/(B\cos(\theta))$ where t is thickness of crystallite, K is a crystallite shape dependent constant, λ is X-ray wavelength, B is FWHM (full width at half max) or integral breadth, $B = (2\theta$ high$)-(2\theta$ low), and θ is Bragg angle, the average grain size of 12, 15, and 24 nm have been obtained for as-deposited and the samples annealed at 300 and 450 °C, respectively. On the other hand, using the Vegard's law for these samples, the Zn concentration x of 0.36, 0.44, and 0.41 has been obtained, respectively. We note that the Vegard's law and Scherrer formula, which strongly depend on the peak position and FWHM of the diffraction peaks, roughly estimates Zn concentration and average size of the grains since other parameters like micro and macro strains and/or formation of other phases affect peak parameters. For example, the sample annealed at 450 °C possess a Zn concentration value which is lower than that of the sample annealed at 300 °C. We attribute this to the out diffusion of Zn atoms or formation of other phases besides the CdZnTe phase, even though these secondary phases are not detectable by XRD method. We will study this feature in detail by other characterization techniques like EDS and XPS measurements. The other feature is the appearance of a shoulder in the lower 2θ side of the (1 1 1) diffractions of the as-deposited sample shown in Fig. 1(b). This shoulder is reduced in the annealed samples as a result of enhanced crystallization. We attributed the observed

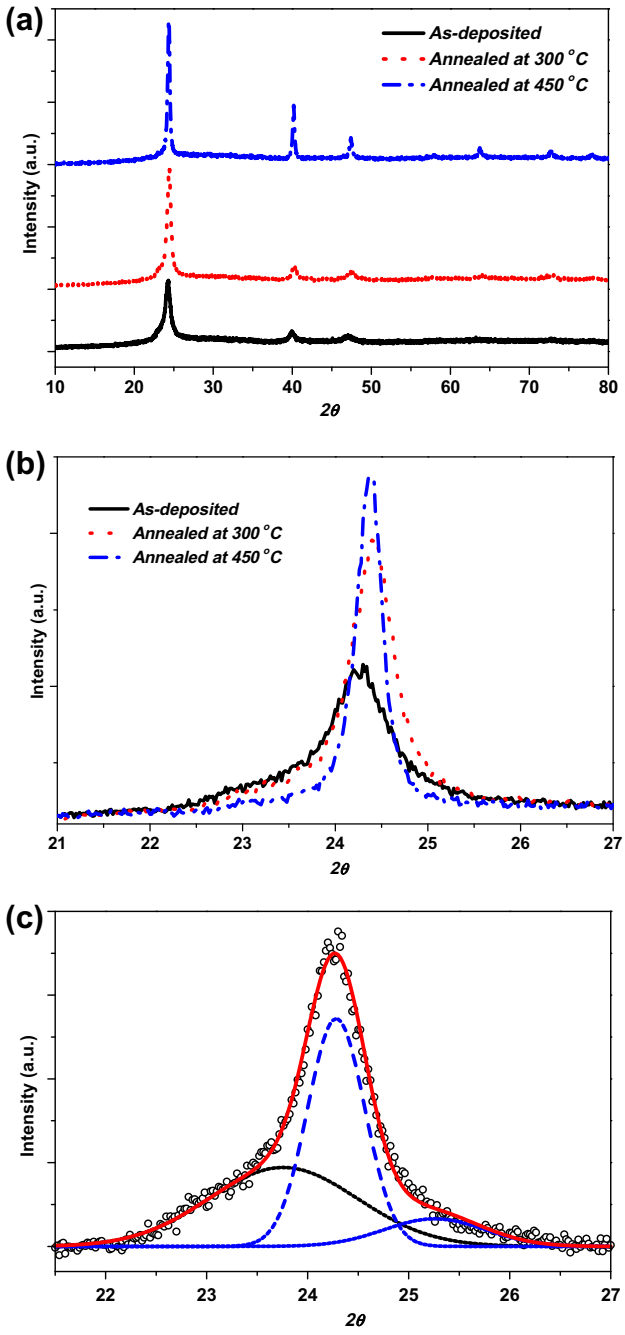

Fig. 1. Influence of annealing on the XRD spectra of the $Cd_{1-x}Zn_xTe$ samples prepared at substrate temperature of 400 °C and post annealing at 300 and 450 °C in the range of 10–80° (a), position and relative evolution of (1 1 1) diffraction peaks (b), decomposed spectra of the (1 1 1) diffraction peak of the as-deposited sample (c).

shoulder to the amorphous CdTe portion. Hence, the (1 1 1) diffraction peak of the as-deposited sample is well fitted by two broad Gaussian components at 23.76° and 25.26° and relatively sharp Gaussian component at 24.28° in which we related them to the amorphous CdTe, ZnTe and crystalline $Cd_{0.64}Zn_{0.36}Te$, respectively (see Fig. 1(c)).

3.2. SEM and EDS results

In order to obtain information about surface morphology and elemental composition of the $Cd_{1-x}Zn_xTe$ alloys, scanning electron microscopy (SEM) and energy dispersive X-ray spectroscopy (EDS)

measurements have been performed. Fig. 2 shows the influence of annealing treatments on the SEM images of the $Cd_{1-x}Zn_xTe$ alloys. Compared to the as-deposited sample in which regions with light gray contrast correspond to the rough surfaces exist (Fig. 2(a)), the sample annealed 300 °C has a very uniform and compact morphology (Fig. 2(b)). Fig. 2(c and d) compare the SEM images of the samples annealed at 300 and 450 °C. While two samples posses a very close-packed nanograins, in the sample annealed at 450 °C, dark gray contrast regions correspond to hole like features can be seen. These features with diameters smaller than 50 nm observable as dark spots in Fig. 2(e) are different from very large dark features with sizes about 10 μm (Fig. 2(f)). They were identified as Te precipitates and inclusions and their role has been under discussion since the introduction of the CdZnTe detectors as a room-temperature x- and gamma-ray detector. Te precipitates are a consequence of the retrograde solid solubility of tellurium during cooling to room temperature, including a nucleation process. On the other hand, Te inclusions in CdTe or CdZnTe crystals originate at the growth interface. Te-rich droplets are trapped at the boundary layer of the interface as a consequence of morphological instability of the liquid–solid interface during growth.

By EDS measurements, we can obtain the elemental concentration, zinc concentration (x) and stoichiometry (s) of the as-deposited and annealed $Cd_{1-x}Zn_xTe$ alloys and monitor these values from different parts of the sample. Table 1 summarizes the results obtained by XRD and XPS measurements. For example, in the sample annealed at 450 °C in Fig. 2(e) the EDS data measured from light gray regions and dark spots (Te precipitates) and in Fig. 2(f) the large dark region (Te inclusions) the stoichiometry s values of 1.04, 1.09, and 1.14 have been obtained, respectivelly. This result indicates the areas identified as Te precipitates and inclusions are rich in Te which is in agreement with early reported results. We also note that while taking data from dark spots (Fig. 2(e)), a large amount of Si related to the glass substrate has been detected indicating a hole like structure. On the other hand, when taking data from dark region (Fig. 2(f)) a decrease in Si and a large increase in the detected O has been observed, which can be related to the observed TeO_2 feature in XPS spectrum of the Te3d.

When we compare the EDS results with those obtained from XRD measuremets, we see that the x values obtained from the XRD analysis are smaller than those of EDS measurements. We think that there are two main factors that are responsible for this

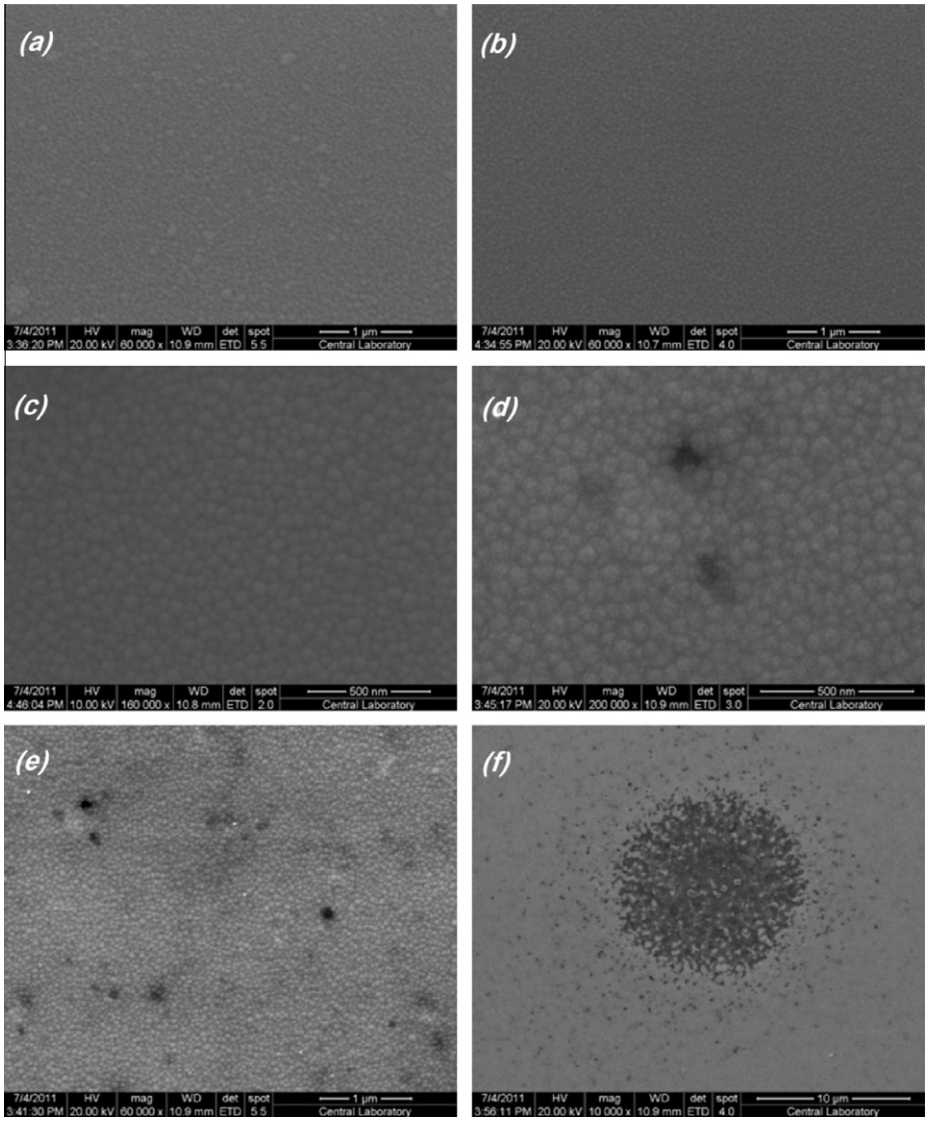

Fig. 2. SEM image of the as-deposited (a) and 300 °C annealed (b) samples, the higher magnification SEM image of the 300 °C (c) and 450 °C (d) annealed samples, and SEM images of the sample annealed at 450 °C in which Te precipitates (e) and Te inclusions (f) are observable.

Table 1
Summary of the structural and optical characterization of the as-deposited and annealed $Cd_{1-x}Zn_xTe$ alloys.

	As-deposited	Annealed at 300 °C	Annealed at 450 °C
Grain size (nm)	12	15	24
x value by XRD	0.36	0.44	0.41
Eg(x) (eV) by UV	1.66	1.65	1.59
x value by Eg(x)	0.24	0.22	0.14
Roughness (nm)	4.88	2.8	3.46 4.6
x value by EDS	0.37	0.40	Light: 0.44 Dark: 0.53 Hole 1 (2): 0.64 (0.80)
s value by EDS	1.12	1.08	Light: 1.04 Dark: 1.09 Hole 1 (2): 1.05 (1.14)
x value by XPS	1st sputter: 0.38 Average of 4 sputter: 0.37 Average of depth profile: 0.373	1st sputter: 0.36 Average of 4 sputter: 0.344 Average of depth profile: 0.361	1st sputter: 0.88 Average of 4 sputter: 0.54 Average of depth profile: 0.402
s value by XPS	1st sputter: 1.30 Average of 4 sputter: 1.30 Average of depth profile: 1.30	1st sputter: 1.271 Average of 4 sputter: 1.293 Average of depth profile: 1.276	1st sputter: 0.32 Average of 4 sputter: 0.90 Average of depth profile: 1.116

result. First one is related to the micro strains or local strains on the nanograins (such as compressive stress) which results in the shift of $Cd_{1-x}Zn_xTe$ XRD diffraction peaks giving raise to differet *x* values. The other factor is related to the formation of other zinc containg phases like ZnO beside $Cd_{1-x}Zn_xTe$ phase. For example in the SEM image of the sample prepared at substrate temperature of 400 °C and annealed at 300 °C (the upper image in Fig. 2), clusters of small grains are observable on the surface. On the XRD spectra of this sample a feature appeared at 2θ value of ~38.5° (not shown here) which has been reported as evidence of zinc oxide diffraction. For this sample by XRD data the value of $x = 0.27$ has been obtained, which is smaller than thats of EDS measurements ($x = 0.44$). On the other hand, for the sample prepared at substrate temperature of 400 °C and annealed at 300 °C (the lower SEM image in Fig. 2) the *x* value obtained by XRD measurement ($x = 0.43$) is very close to that of EDS measurements ($x = 0.41$). This sample which belongs to the set deposited at higher substrate temperature of 400 °C, have good morphology and particularly the surface of the film is uniform. This homogenity and data accordance between XRD and EDS measurements could be due to the applied higher substrate temperature, which can lead to the increase of the kinetic energy of the sputtered particles, causes to the increase of the mobility of particles in the surface of the film. Then, particles can migrate to more suitable lattice sites and adjust their own bond direction and length to obtain optimum bonding to the adjacented ones, which are helpful for nucleation and growth, and consequently improved the crystallinity.

3.3. AFM measurements

To study the surface morphology of the $Cd_{1-x}Zn_xTe$ alloys and its evolution by annealing treatments in details, AFM measurements have been performed. Fig. 3(a and b) present three dimensional AFM images of the as-deposited sample. The surface forms a hillock structure and the maximum height and diameter are about 20 and 100 nm, respectively. The root-mean-square (RMS) surface roughness is 4.88 nm, and the grain boundaries are unconspicuous, which is likely due to the existence of non-crystalline or amorphous portion. As confirmed by XRD measurements, the as-deposited sample in which deposited at substrate temperature of 400 °C includes crystalline $Cd_{0.64}Zn_{0.36}Te$ phase together with mostly CdTe amorphous phase. The AFM phase profile is shown in Fig. 3(c), and it implies the existence of two different phases in the system. We speculate that the grain boundaries with dark contrast to be amorphous CdTe, since their contribution are reduced in the annealed samples like the observed reduction in the relative contribution of amorphous CdTe in the XRD spectra. In addition, we notice that there exist a number of hole like features most evident in Fig. 3(d) and are detailed in AFM line profile. The typically shown hole has a peak to valley distance of 53 nm and a depth of about 12 nm. As discussed in previous section, these features are attributed to Te precipitates and prefer the grain boundaries as nucleation sites. When a crystal shows a high density of Te precipitates e.g., along grain boundaries extending from one electrode to another, it results in a very high leakage current and poor spectrometric performance throughout the region with clusters of Te precipitates.

Fig. 4(a and b) show the three dimensional AFM images of the sample annealed at 300 °C. Compared with as-deposited sample, the surface is more uniform and the surface RMS roughness (2.8 nm) has reduced significantly. The grains are more close-packed, and their size distribution has been decreased. Fig. 4(c) presents a line profile taken from topographic AFM image. As can be seen by post deposition annealing at 300 °C, the number of hole like features has been decreased and their peak to valley distance and depth decreased as well. On the other hand, for the sample annealed at 450 °C, although most part of the surface is similar to the sample annealed at 300 °C (Fig. 4(e) with RMS roughness of 3.46 nm) there are two features affecting the film uniformity and performance. One is discussed in previous section as Te inclusions, and the other is particulates typically 120 nm in diameter and 150 nm in height. Taking the particulated one into the account, the RMS roughness of 4.6 nm has been obtained (Fig. 4(d)). Furthermore the grain boundaries are not as conspicuous as that of the sample annealed at 300 °C, and the number and depth of the hole like features have been increased. So, the film deposited at substrate temperature of 400 °C and post annealed at 450 °C posses a surface with good uniformity and significantly low RMS roughness value which could be a well candidate for further film preparation in devices for solar cell and gamma-ray detectors.

3.4. XPS measurements

XPS was used to monitor the changes in chemical composition and possible oxidation of each element on the surface and underlying layers, and to identify the changes in the stoichiometry *s* of the as-deposited and annealed samples. After four times sputtering with 2000 eV Ar^+ ions with the cycle of 2 min followed by 4 min 3500 eV sputtering cycles, the steady state elemental composition values was obtained for each element. The primary peaks of

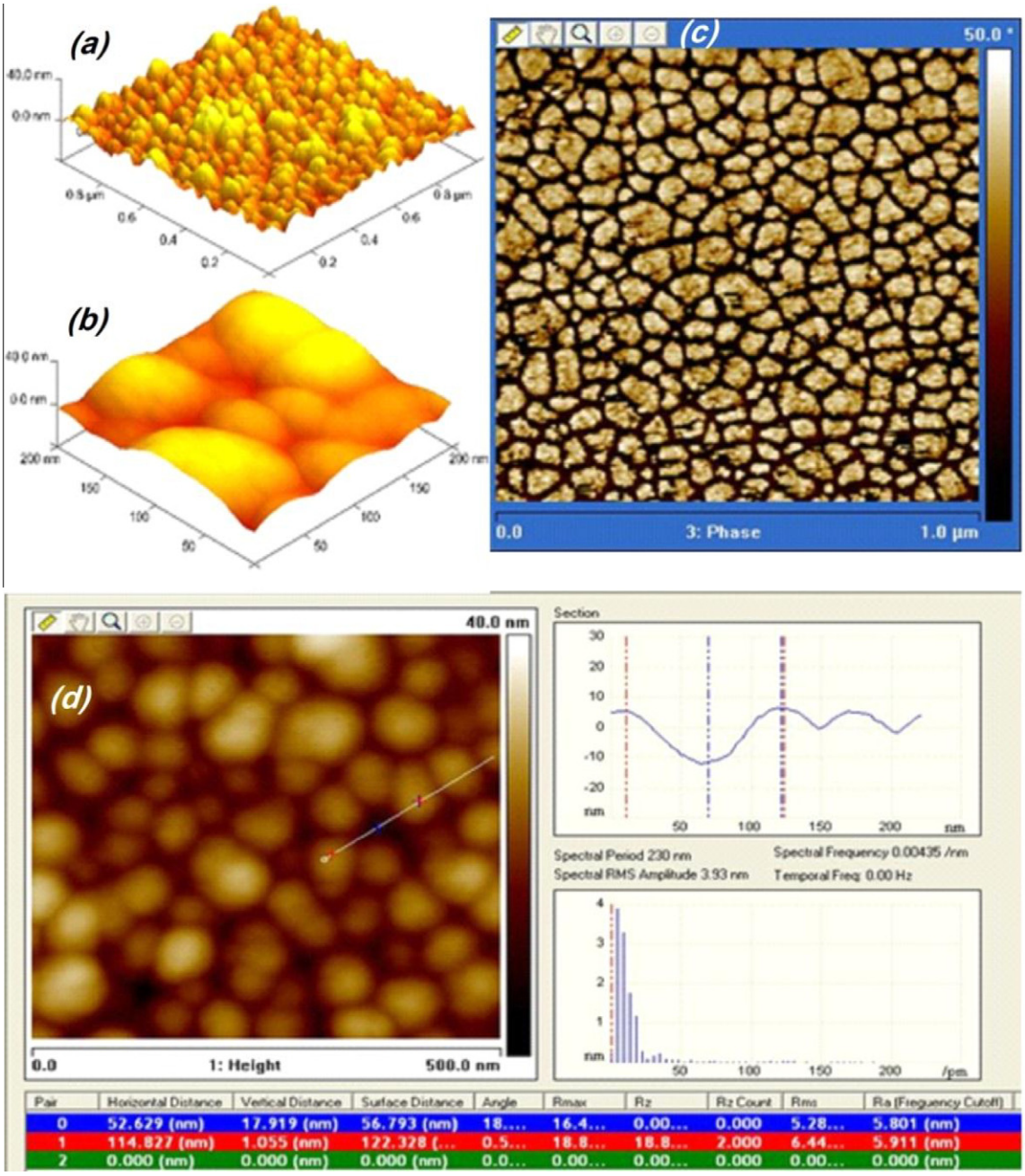

Fig. 3. Three dimensional AFM images of the as-deposited $Cd_{1-x}Zn_xTe$ films (a) and (b), the phase profile (c) and line profile (d) of the sample.

interests, O 1s, C 1s, Te 3d, Cd 3d, and Zn 2p were scanned individually to optimize their spectral intensity and resolution. The O 1s line and the C 1s lines were routinely scanned to establish the presence of oxides and contamination. The spectral shift was corrected using the measured C 1s peak, by supposing a binding energy of 284.6 eV, and Cd 3d5/2 (B.E. = 405.1 eV) was used to check the beam energy for the surface without carbon. All of the curves were fitted with Gaussian functions after subtracting a Shirley background and the corresponding integrated intensities were recorded.

Fig. 5(a–c) demonstrate the integrated intensities of the Cd, Zn, Te, and O obtained by 25 sputtering cycles from as-deposited and annealed $Cd_{1-x}Zn_xTe$ samples. As can be seen, for the as-deposited sample the integrated intensity of all elements is almost the same and does not change by Ar sputtering implying homogeneous distribution of the atoms on the surface and underlying layers. So, the Zn concentration (x = [Zn]/([Zn]+[Cd])) and film stoichiometry (s = [Te]/([Zn]+[Cd])) fairly fluctuate near the values of 0.37 and 1.3, respectively (Fig. 5(d)). We note that the obtained value for x is in well agreement with values obtained by XRD (0.36) and EDS (0.37) measurements. The calculated values for x and s after first sputtering, the average of first 4 sputtering, and the average of 25 sputtering cycles are presented in Table 1. For the sample annealed at 300 °C while the integrated intensities of Cd, Zn, and Te after first six sputtering cycles show considerable decrease (compared with the as-deposited sample), that of O has been increased. This implies oxidation of the surface, and in following we will discuss the possible oxide species. The obtained values for x and s are slightly lower than those of as-deposited sample (Table 1). For sample annealed at 450 °C, the situation is quite different. The

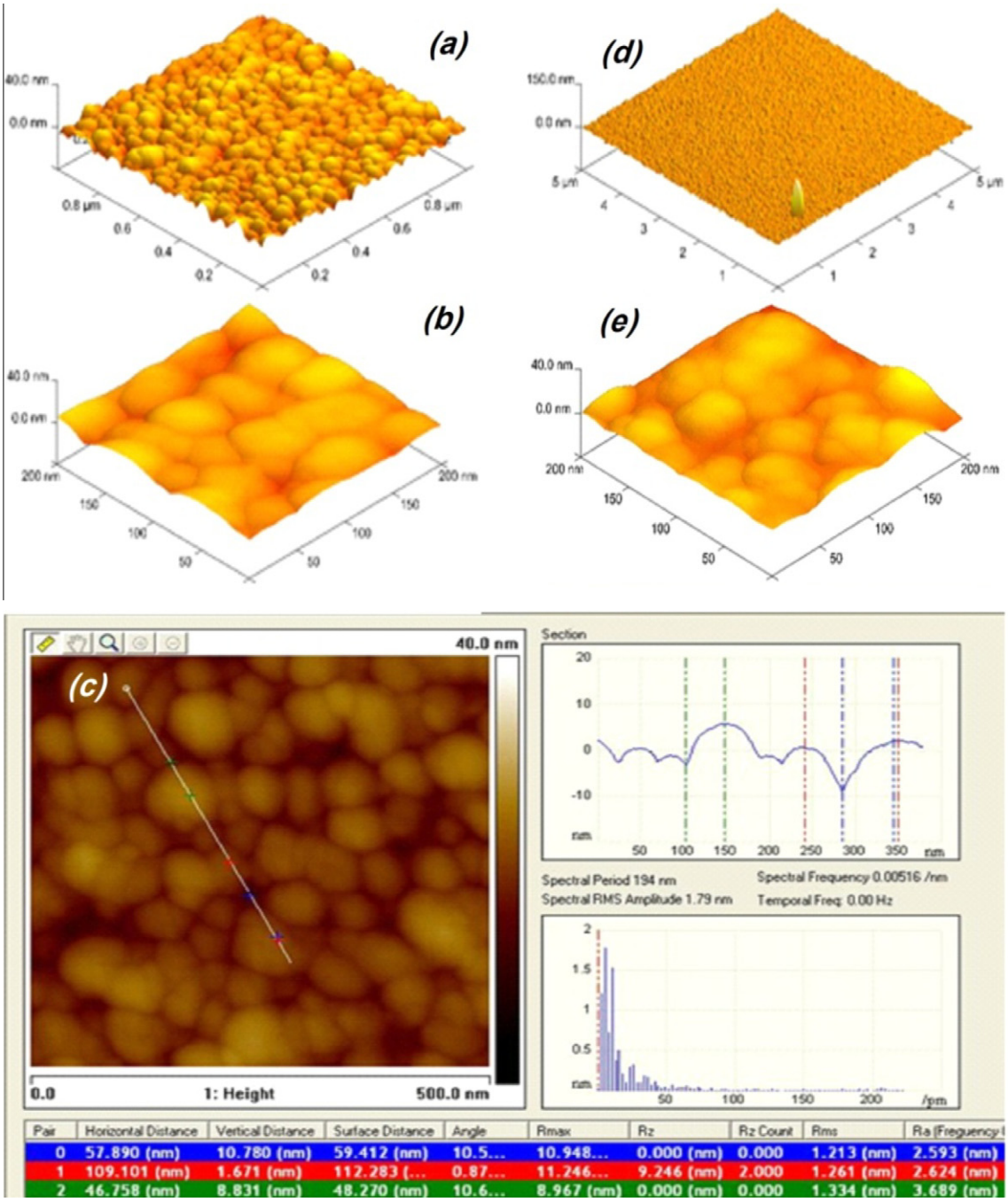

Fig. 4. Three dimensional AFM images of the 300 °C annealed $Cd_{1-x}Zn_xTe$ films (a) and (b), and its line profile (c), and the three dimensional AFM images of the 450 °C annealed $Cd_{1-x}Zn_xTe$ films (d) and (e).

observed increase in the integrated intensity of O and decrease in that of Cd and Te after intial sputtering cycles is more pronounced in the sample annealed at higher temperature of 450 °C. Furthermore, a drastic increase in the integrated intensity of Zn 2p has been observed in the layers near to the surface. So as can be seen from Fig. 5(c), the surface of the film is rich in Zn and O atoms. This leads to the large difference for x and s values obtained from layers near to the surface and that is from deep lying layers. These values are $x = 0.88$ and $s = 0.32$ after 1st sputtering and are $x = 0.28$ and $s = 1.29$ after 20th sputtering. We note that while the obtained value for stoichiometry of s after 20th spttering is almost the same with that of as-deposited and 300 °C annealed samples, the Zn concentration of x after 20th sputtering (0.28) is about 25% lower than those of as-deposited and 300 °C annealed samples (0.37). This means that, even at deep lying layers, there is a considerable decrease in the Zn concentration. This lack of Zn in deeper layers and its abundance in the region near the surface can be interpreted as the surface segragation of Zn atoms in the sample subjected to the higher annealing temperature of 450 °C.

To study possible oxidation and surface morphology of the $Cd_{1-x}Zn_xTe$ films upon annealing, the O 1s peak is decomposed to four components located at 529.6, 530.5, 531.1, and 532.4 eV corresponding to the CdO, ZnO, TeO_2/$CdTeO_3$, and C contamination and/or $Cd(OH_2)$, respectivelyas shown in Fig. 6. Sometimes, the O 1s peak is more generally resolved into two peaks: one peak with a lower binding energy (between those of CdO and Te oxides) from

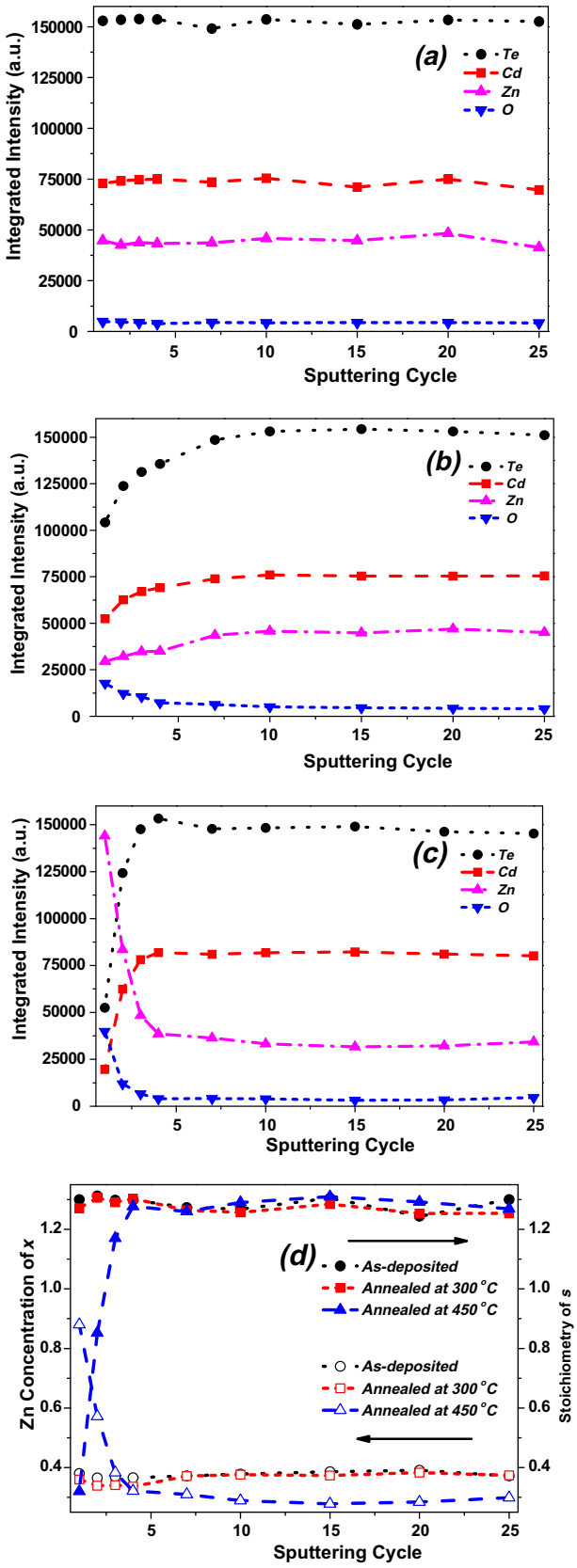

Fig. 5. Integrated intensities of the Cd, Zn, Te, and O elements after 25 sputtering cycles for as-deposited sample (a), the samples annealed at 300 °C (b), and 450 °C (c). The variation of Zn concentration of x and stoichiometry of s by annealing treatment (d).

ions with the formal valence state O_2, the other higher binding energy component located at 532.3–532.5 eV attributed to the presence of loosely bound oxygen on the surface of the film such as CO_3, adsorbed H_2O or adsorbed O_2. From a chemical standpoint, one expects that Cd oxidizes mainly as $Cd(OH)_2$ and CdO, and Te as TeO_2. In general, Te oxides give rise to a well-resolved peak at higher energies in the Te 3d spectrum. It has been reported that the oxidation of Te to form TeO_2 causes a chemical shift of ~3.2 eV and that of CdTe to form $CdTeO_3$ causes a ~3.5 eV shift. Investigation of Cd oxides from Cd 3d core-level spectrum impossible by the fact that Cd oxides are completely unresolved. Moreover, when Cd is oxidized to form $CdTeO_3$, there is no change in its chemical state and no chemical shift, but only line width broadening. $CdTeO_3$ was proposed as the most stable phase among several other oxide phases predicted based on the equilibrium phase diagram of the Cd–Te–O system. On the other hand, decomposition of Zn 2p spectrum into two peaks at 1021.5 and ~1022 eV has been reported and are assigned to bulk crystal and ZnO, respectively. The core level shift of Te and Zn after oxidation are due to the charge density transfer from Te and Zn to O atoms.

Fig. 6(a) demonstrates the O 1s spectrum of the as-deposited and annealed $Cd_{1-x}Zn_xTe$ samples, monitored from the surface and after 2th and 20th sputtering cycles. As can be seen, the intensity of the O 1s spectrum gathered from the surface of the sample enhanced strongly in annealed samples. Furthermore, its intensity decreases when data collected from deep lying layers. Also depending on the annealing treatment and depth of the sputtering cycle,the position of the whole O 1s peak and relative contribution of the Cd, Zn, and Te oxides changes. To understand the relative contribution of these oxides, the decomposed spectra of the as-deposited and annealed samples at 300 and 450 °C are demonstrated in Fig. 6(b–d). In that of as-deposited sample in which is weakly oxidized (Fig. 6(b)), all Cd, Zn, and Te atoms takes equally part in the oxidation process. For the sample annealed at 300 °C, the $Cd(OH)_2$ and/or CO related peak located 532.36 eV is the dominant feature of the spectrum (Fig. 6(c)). In the case of high temperature annealing at 450 °C, Te containing compounds ($CdTeO_3$, or TeO_2) are more pronounced as can be seen in Fig 6(d).

3.5. Band gap of the deposited $Cd_{1-x}Zn_xTe$ films

The transmission spectra in the region of the optical absorption band edge were measured for as-deposited and heat-treated at 300 and 450 °C $Cd_{1-x}Zn_xTe$ samples. The optical absorption coefficient (α) was calculated from the transmittance using the following relation $\alpha = (1/d)\ln(100/T)$, where T is the transmittance and d is the thickness of the crystal. As a direct band gap semiconductor, the crystal under study has an absorption coefficient (α) obeying the following relation for high photon energies ($h\nu$): $(\alpha h\nu) = A(E_g - h\nu)^2$, where E_g is the optical band gap of the crystal, and A is a constant.

According to the expression $(\alpha h\nu) = A(E_g - h\nu)^2$, it should be possible to fit portions of $\alpha h\nu = f(h\nu)$ curves to one or more of the standard dependences, namely $(\alpha h\nu)^2 = f(h\nu)$ for allowed direct transitions, $(\alpha h\nu)^{2/3} = f(h\nu)$ for forbidden direct transitions, and $(\alpha h\nu)^{1/2} = f(h\nu)$ for indirect transitions. The analysis of our experimental results, (Fig. 7) shows that the best fit is obtained for $(\alpha h\nu)^2 = f(h\nu)$ curves which have a linear portion. Consequently, these curves have been used for the estimation of the band gap values [22–26]. The optical band gaps have been estimated as 1.66, 1.65 and 1.59 eV for as-deposited and annealed at 300 and 450 °C samples, respectively. We see that the annealing causes the band gap to decrease slightly. The further decrease of the optical band with increasing annealing temperature may be due to the

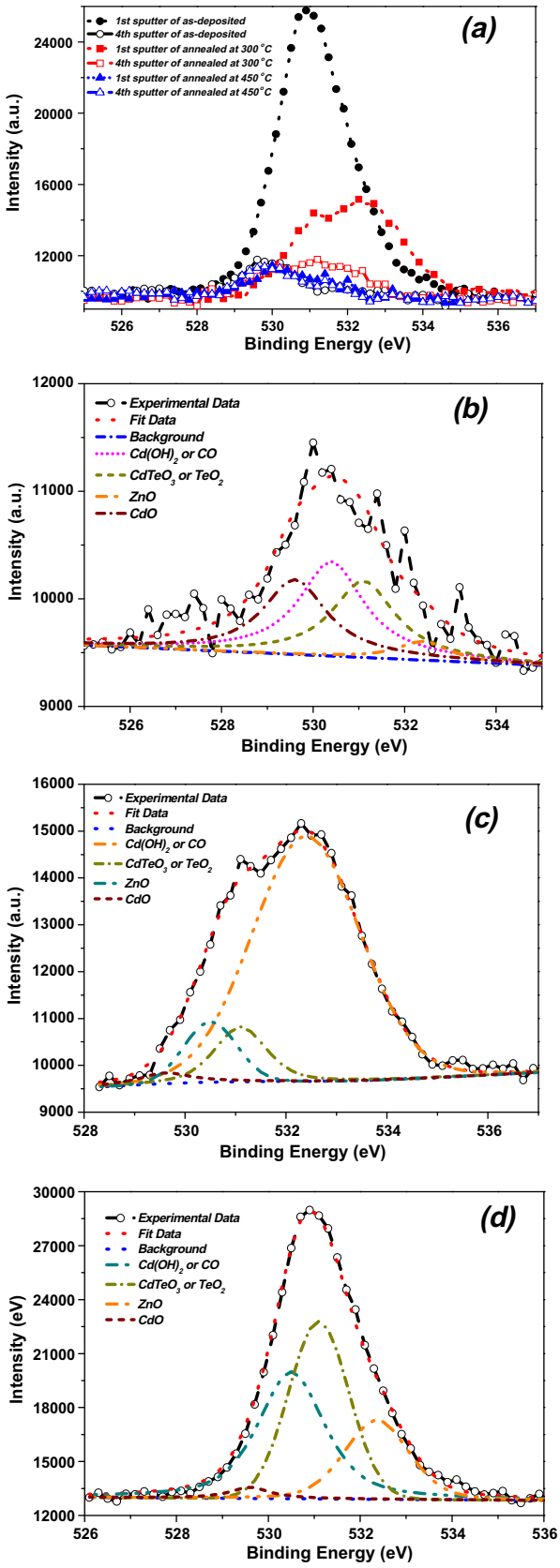

Fig. 6. Comparison of O 1s profile after 1st and 4th sputtering cycle of the as-deposited and annealed samples (a), deconvoluted O 1s spectra of the as-posited sample (b) and the samples annealed at 300 °C (c) and 450 °C (d) after 1st sputtering cycle. The inset in (d) shows the TeO_2 related component in the Te spectrum after 1st sputtering cycle of the sample annealed at 450 °C.

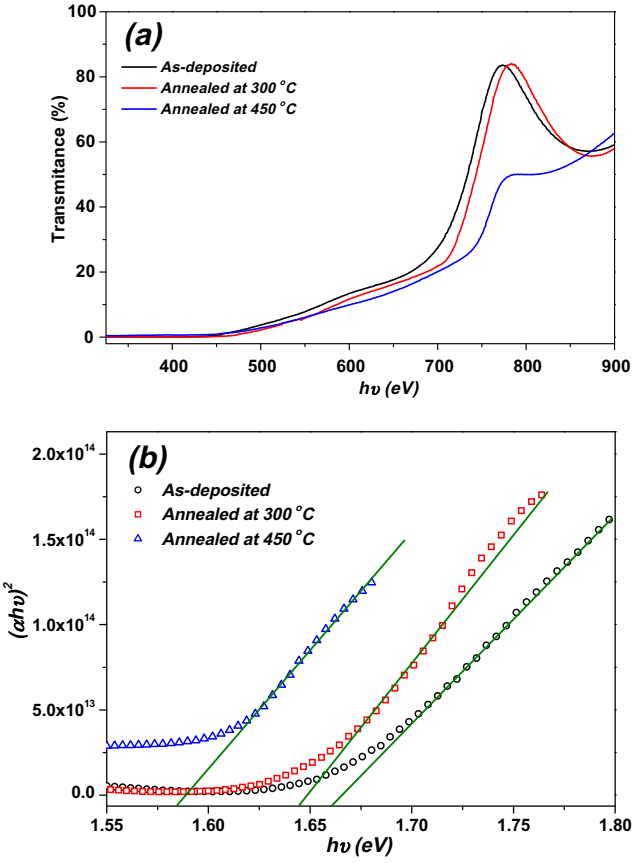

Fig. 7. (a) Transmission spectra of as-deposited and annealed at 300 and 450 °C samples. (b) $(\alpha h\nu)^2$ versus $h\nu$ to determine the optical band gap of as-deposited and annealed at 300 °C and 450 °C samples.

remaining free tellurium in the films. Their unsaturated bonds and other structural defects can introduce localized states in the forbidden band that can be responsible for narrowing of the band gap [27–29].

4. Conclusions

$Cd_{1-x}Zn_xTe$ thin films were deposited onto heated glass substrates in vacuum by a single target sputtering technique. By deposition of $Cd_{1-x}Zn_xTe$, nanolayered $Cd_{1-x}Zn_xTe$ structures with uniform content at about 200 nm were obtained. By changing the exploration settings homogenous $Cd_{1-x}Zn_xTe$ thin films can be obtained. Depending on preparation conditions and heat treatment, the optical band gap of respective films can be tuned from 1.59 to 1.66 eV. Results show that $Cd_{1-x}Zn_xTe$ thin film sputtered at 400 °C and annealed at 450 °C under the N_2 gas environment indicates the desired behavior.

The results are devoted to the morphology and structure of nanostructured films of such promising material as $Cd_{1-x}Zn_xTe$ can be useful for experts and researchers. Such grown films have also wide applications of the semiconductor in various optoelectronic devices. Further works in this area are on the way to improve the performance of the film and its applications in photovoltaic and imaging devices.

Acknowledgements

The author wish to thank Middle East Technical University for their generous support.

This work is supported by Abant Izzet Baysal University under contract number: AIBU-BAP.2009.03.02.319. and by Ministry of Development of Turkey under the contract number 2012K120360.

References

[1] M. Dammak, S. Alaya, A. Zerrai, G. Bremond, R. Triboulet, Semicond. Sci. Technol. 12 (1997) 600.
[2] G.G. Rusu, M. Rusu, J. Optoelectron. Adv. Mater. 7 (2) (2005) 885.
[3] N. Chaure, A.P. Samantilleke, I.M. Dharmadasa, Sol. Energy Mater. Sol. Cells 77 (3) (2003) 303.
[4] V. Valdna, Thin Solid Films 387 (1–2) (2001) 192.
[5] J. Malzbender, E.D. Jones, N. Shaw, J.B. Mullin, Semicond. Sci. Technol. 11 (5) (1996) 130.
[6] H. Bayhan, C. Ercelebi, Semicond. Sci. Technol. 12 (1997) 600–608.
[7] M. Dammak, S. Alaya, A. Zerrai, G. Bremond, R. Triboulet, Semicond. Sci. Technol. 13 (1998) 762–768.
[8] J.H. Dinan, S.B. Qadri, J. Vac. Sci. Technol. A 3 (1985) 851.
[9] B. Pellicary, J.P. Chamonal, G.L. Destefanis, L. DiCiocio, Proc. SPIE 865 (1988) 22.
[10] M. Basol, V.K. Kapur, M.L. Ferris, J. Appl. Phys. 66 (1989) 1816.
[11] J. Gonzales-Hernandes, O. Zelaya, J.G. Mendoza-Alvares, E. Lopez-Cruz, D.A. Pawlick, D.D. Alred, J. Vac. Sci. Technol. A 9 (1991) 550.
[12] A. Aydinli, A. Compan, G. Contreras-Puente, A. Mason, Solid State Commun. 80 (1991) 465.
[13] K.H. Kim, Y.H. Na, Y.J. Park, T.R. Jung, S.U. Kim, J.K. Hong, IEEE Trans. Nucl. Sci. 51 (2004) 3094.
[14] K. Phabakar, S.K. Narayandass, D. Mangalaraj, J. Alloys Compd. 364 (2004) 23.
[15] G.G. Rusu, J. Optoelectron. Adv. Mater. 8 (2006) 931.
[16] G.G. Rusu, M. Rusu, M. Girtan, Vacuum 81 (2007) 1476.
[17] T.L. Chu, S.S. Chu, C. Ferekides, J. Britt, J. Appl. Phys. 71 (1992) 5635.
[18] M. Becerril, H. Silva-Lopez, O. Zelaya-Angel, Rev. Mex. Fis. 50 (2004) 588.
[19] R. Sharma, L. Dori, S. Chandra, K. Misra, Proc. SPIE 3975 (2000) 1278.
[20] A. Haloui, Y. Feutelais, B. Legendre, J. Alloys Compd. 260 (1997) 179.
[21] V.N. Guskov, J.H. Greenberg, M. Fiederle, K.W. Benz, J. Alloys Compd. 371 (2004) 118.
[22] D. Lucaa, L.S. Hsu, J. Optoelectron. Adv. Mater. 5 (4) (2003) 835–840.
[23] G.I. Rusu et al., J. Macromol. Sci. R, Part B: Phys. 48 (2009) 238–253.
[24] N. Tigau, Cryst. Res. Technol. 42 (2007) 281–290.
[25] Chu-Chi Ting et al., J. Appl. Phys. 88 (8) (2000) 4628–4633.
[26] C. Baban, Y. Toyoda, M. Ogita, J. Optoelectron. Adv. Mater. 7 (2005) 891.
[27] M. Rusu, G.G. Rusu, Phys. Low-Dimensional Struct. 3 (4) (2002) 105–116.
[28] R. Chakrabarti, S. Ghosh, S. Chaudhuri, A.K. Pal, J. Phys. D Appl. Phys. 32 (1999) 1258–1268.
[29] M. Becerril, H. Silva-Lopez, O. Zelaya-Angel, Rev. Mex. Fis. 50 (2004) 588–593.